Energy Equip. Sys./ Vol. 6/No. 2/June 2018/ 143-154

ENERGY EQUIPSYS

Energy Equipment and Systems

http://energyequipsys.ut.ac.ir
www.energyequipsys.com

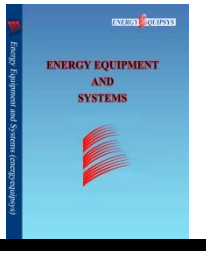

Numerical study of natural convection heat transfer of Al_2O_3/Water nanofluid in a Γ-shaped microchannel

Authors

Amireh Nourbakhsh[a*]
Morteza Bayareh[b]

[a] Department of Mechanical Engineering, Bu-Ali Sina University, Hamedan, Iran

[b] Department of Mechanical Engineering, Shahrekord University, Shahrekord, Iran

Article history:

Received : 31 October 2017
Accepted : 7 January 2018

ABSTRACT

Finite-volume procedure is presented for solving the natural convection of the laminar $Al_2O_3/Water$ nanofluid flow in a Γ shaped microchannel in this article. Modified Navier-Stokes equations for nanofluids are the basic equations for this problem. Slip flow region, including the effects of velocity slip and temperature jump at the wall, are the main characteristics of flow in the slip flow region. Steady state equations were solved by using time marching method. In provided FORTRAN code, the finite volume method and an explicit fourth-order Runge–Kutta integration algorithm were applied to find the steady state solutions. Also an artificial compressibility technique was used to couple the continuity to the momentum equations as it is simpler and converges faster. The Grashof numbers from 10^2 to 10^5 were considered. The results showed that Nusselt number increases with the Grashof number and the parameter R (the ratio of minimum diameter of nanoparticles and maximum one).. As the parameter R increases, the distortion of the isotherm lines increases to some extent.

Keywords: Microchannel, Velocity Slip, Temperature Jump, Grashof Number, Nanoparticle.

1. Introduction

Fluid flow and heat transfer inside the microchannels play an important role in many engineering tools such as micro-pumps, micro-valves and micro-sensors. On the other hand, advance electronic device is highly dependent on development of devices providing high heat transfer in small sizes. Nevertheless, low heat transfer coefficient of fluids such as water, alcohol and ethylene glycol has caused a serious obstacle for this goal. To overcome this problem, increasing interest has been raised to study fluids heat transfer improvement. One of the solutions is to add solid particles to the fluid. Recently, numerous studies have addressed natural heat transfer in containers. Dagtekin and Oztop studied natural convection heat transfer in a square-shape container including two heated sections by means of finite volume method. They studied the effect of heated sections location and their height on heat transfer and fluid flow. They also used a simple method and

* Corresponding author: Amireh Nourbakhsh
Department of Mechanical Engineering, Bu-Ali Sina University, Hamedan, Iran
Email: nourbakhsh@basu.ac.ir

solved the equations by iteration and application of Tomas algorithm. They found that Nusslet number will increase with increase in heater length; but heaters location has lower impact on heat transfer and Nusslet number [1]. In contrast, addition of solid particles has been recognized as one of the solutions for improving thermal properties of base fluid. For instance, addition of aluminum oxide particles (mean diameter of 13 nm) to water with volume percentage of 4.3% can increase the thermal properties for about 30% [2]. Numerous experimental studies have proven that application of nanoparticles can significantly enhance the thermal properties of the fluid [3-7]. Zhang et al. showed that adding nanoparticles to water will result in increase in Nusslet number [8]. Arie et al. investigated the heat transfer in micro-dimensional heat exchanger [9]. Ebrahimi et al. numerically investigated heat transfer and fluid flow inside rectangular microchannels [10]. Yue et al. studied heat transfer inside a micro-dimensional manifold. Their results showed that increase in volume fraction of nanoparticles will lead to increase in Nusslet number [11]. Hedayati et al. also addressed the effect of nanoparticles shape on heat transfer of water-TiO_2 inside a circular microchannel [12]. Zou et al. examined laminar flow of water-ethylene glycol-Al_2O_3 in a thermal blade [13]. Yang et al. studied heat transfer in three types of nanofluids (water-copper, water aluminum oxide and water-copper oxide) in wavy microchannel. Their results showed that application of nanofluid will enhance heat transfer [14].

Numerous studies have been conducted on microchannel and nanofluids; however, heat transfer and nanofluid flow inside a Γ-shape microchannel has not been addressed yet. On the other hand, generalization of the results of macrochannels to microchannels may give rise to a huge error. Therefore, this paper is aimed to study this problem.

2. Problem

In this article, nanofluid flow and natural convection heat transfer will be studied in a Γ-shape microchannel filled with water-aluminum oxide nanofluid. Fig. 1 shows a microchannel along with boundary conditions. Velocity slip and temperature jump boundary conditions were considered in the walls. To reduce the computation time, regular and staggered grid was used to produce grid. Jimson finite volume method has been widely used in many studies due to its simplicity [15]. In this study, for discretization of convection and viscose terms, second order finite volume method was applied. For explicit discretization of temporal terms, the fourth-order Runge–Kutta method was employed. An artificial compressibility technique was used for association of continuity equations to momentum equations [16, 17].

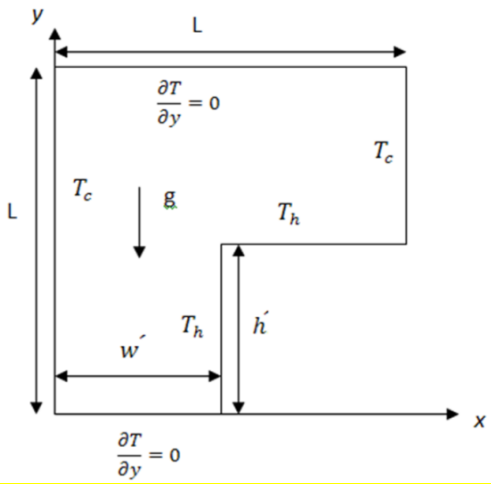

Fig. 1. Illustration of problem with boundary condition.

3. Governing Equations

Physical properties of fluid flow can be controlled by three basic equations: mass, momentum and energy conservation equations.

Mass conservation equation

$$\frac{\partial \rho}{\partial t}+\frac{\partial u}{\partial x}+\frac{\partial v}{\partial y}+\frac{\partial w}{\partial z}=0 \tag{1}$$

Momentum conservation equation

$$u\frac{\partial u}{\partial x}+v\frac{\partial u}{\partial y}+w\frac{\partial u}{\partial z}=g_x-\frac{1}{\rho}\frac{\partial p}{\partial x}+\frac{\mu}{\rho}\left(\frac{\partial^2 u}{\partial x^2}+\frac{\partial^2 u}{\partial y^2}+\frac{\partial^2 u}{\partial z^2}\right)$$

$$u\frac{\partial v}{\partial x}+v\frac{\partial v}{\partial y}+w\frac{\partial v}{\partial z}=g_y-\frac{1}{\rho}\frac{\partial p}{\partial y}+\frac{\mu}{\rho}\left(\frac{\partial^2 v}{\partial x^2}+\frac{\partial^2 v}{\partial y^2}+\frac{\partial^2 v}{\partial z^2}\right) \tag{2}$$

Energy conservation equation

$$u\frac{\partial T}{\partial x}+v\frac{\partial T}{\partial y}+w\frac{\partial T}{\partial z}=$$
$$\alpha\left(\frac{\partial^2 T}{\partial x^2}+\frac{\partial^2 T}{\partial y^2}+\frac{\partial^2 T}{\partial z^2}\right) \quad (3)$$
$$\alpha=\frac{k}{\rho c_p}$$

Dimensionless form of nanofluid equations have the following form:

Continuity equation:

$$\frac{\partial U}{\partial X}+\frac{\partial V}{\partial Y}=0 \quad (4)$$

Momentum equation along x direction

$$\frac{\partial U}{\partial \xi}+U\frac{\partial U}{\partial X}+V\frac{\partial U}{\partial Y}=$$
$$\frac{-\rho_f}{\rho_{nf}}\frac{\partial P}{\partial X}+\frac{\mu_{eff}\,Pr}{\rho_{nf}\nu_f}\left(\frac{\partial^2 U}{\partial X^2}+\frac{\partial^2 U}{\partial Y^2}\right) \quad (5)$$

Momentum equation along y direction:

$$\frac{\partial V}{\partial \xi}+U\frac{\partial V}{\partial X}+V\frac{\partial V}{\partial Y}=\frac{-\rho_f}{\rho_{nf}}\frac{\partial P}{\partial Y}+$$
$$\frac{\mu_{eff}\,Pr}{\rho_{nf}\nu_f}\left(\frac{\partial^2 V}{\partial X^2}+\frac{\partial^2 V}{\partial Y^2}\right)+ \quad (6)$$
$$\frac{(1-\Phi)\rho_f\bar{\beta}_f+\Phi\rho_s\bar{\beta}_s}{\rho_{nf}\bar{\beta}_f}Pr^2 Gr\theta$$

Energy equation:

$$\frac{\partial \theta}{\partial \xi}+U\frac{\partial \theta}{\partial x}+V\frac{\partial \theta}{\partial Y}=\frac{\alpha_{nf}}{\alpha_f}\left(\frac{\partial^2 \theta}{\partial X^2}+\frac{\partial^2 \theta}{\partial Y^2}\right) \quad (7)$$

The dimensionless equations above were obtained by the following dimensionless parameters:

$$X=\frac{x}{L},\ Y=\frac{y}{L},\ U=\frac{uL}{\alpha_f},\ V=\frac{vL}{\alpha_f},$$
$$\xi=\frac{\alpha_f t}{L^2},\ P=\frac{pL^2}{\rho_f\alpha_f},\ \theta=\frac{T-T_c}{T_h-T_c} \quad (8)$$

Effective viscosity of a fluid containing spherical solid particles was defined by Jang et al. [18] as follows:

$$\mu_{eff}=\mu_f(1+2.5\Phi)\left[1+\eta\left(\frac{d_p}{L}\right)^{-2\varepsilon}\Phi^{\frac{2}{3}}(\varepsilon+1)\right] \quad (9)$$

where, ε and η were considered as -0.25 and 280 for aluminum oxide, respectively. Density:

$$\rho_{nf}=(1-\Phi)\rho_f+\Phi\rho_s \quad (10)$$

For calculation of nanofluid thermal capacity, mixtures law can be employed:

$$(\rho c_p)_{nf}=(1-\Phi)(\rho c_p)_f+\Phi(\rho c_p)_s \quad (11)$$

Thermal diffusion is defined as:

$$\alpha_{nf}=\frac{k_{nf}}{(\rho c_p)_{nf}} \quad (12)$$

Researchers have shown that nanofluid thermal conductivity is a function of thermal conductivity of pure fluid and nanoparticle, nanoparticle shape and volume percent of nanoparticles dispersion. Hamilton, and Crosser [19] first defined thermal conductivity equations of a fluid containing fixed suspended particles as:

$$\frac{k_{stationary}}{k_f}=\frac{k_s+2k_f-2\Phi(k_f-k_s)}{k_s+2k_f+\Phi(k_f-k_s)} \quad (13)$$

Then Xu et al. [20] extended these equations for nanofluids:

$$\frac{k_{nf}}{k_f}=\frac{k_{stationary}}{k_f}+\frac{k_c}{k_f}=$$
$$\frac{k_s+2k_f-2\Phi(k_f-k_s)}{k_s+2k_f+\Phi(k_f-k_s)}+$$
$$c\frac{Nu_p d_f}{Pr}\frac{(2-D_f)D_f}{(1-D_f)^2} \quad (14)$$
$$\frac{\left[\left(\frac{d_{max}}{d_{min}}\right)^{1-D_f}-1\right]^2}{\left(\frac{d_{max}}{d_{min}}\right)^{2-D_f}-1}\frac{1}{d_p}$$

C is a constant, dependent on base fluid properties but independent of nanoparticles type and properties (C is 85 for water and 280 for ethylene glycol). Nu_p is the Nusslet number

of the fluid surrounding the spherical particles which was considered as 2 for water and aluminum oxide. d_f is the molecular diameter of water particles which was considered as 4.5×10^{-10}m. D_f is also defined as:

$$D_f = 2 - \frac{\mathrm{Ln}\Phi}{\mathrm{Ln}\left(\frac{d_{p,min}}{d_{p,max}}\right)} \quad (15)$$

where $d_{p,max}$ and $d_{p,min}$ are maximum and minimum diameter of nanoparticle, respectively.

3.1. Artificial compressibility technique

By development of computational tools, computational fluid dynamics has found a more important role in design and analysis of the systems. In this regard, methods with better convergence rates have gained considerable attention. Generally, compressibility methods have better convergence and have less computational volume in comparison with incompressibility methods. Compressibility methods have been used in many cases only by reducing Mach number for analysis of incompressible flows. Reduction of Mach number was to reduce compressibility effects. Unfortunately, decrease of Mach number will lead to drastic loss of convergence and precision. For solving this problem, artificial compressibility method has been introduced. In this method, by changing the nature of Elliptical–parabolic equations to Hyperbolic – Parabolic equations, it is possible to use compressible methods for incompressible flows. Therefore, artificial compressibility method is one of the most successful methods in simulation of incompressible flows [21]. In this method, a virtual pressure term will be added to continuity equation and hence, the equations of incompressible flow will be converted to hyperbolic form; therefore, ordinary methods of solving compressible flows can be applied. Virtual compressibility method is basically designed for steady flows; however, it was then modified for unsteady problems [22]. The continuity equation by addition of a time-dependent term will be:

$$\frac{1}{\beta}\frac{\partial P}{\partial t} + \frac{\partial U}{\partial X} + \frac{\partial V}{\partial Y} = 0 \quad (16)$$

where β is the artificial compressibility of the fluid.

3.2. Boundary condition

3.2.1. Boundary condition in macro-dimensional channels

For macro-dimensional channels, no slip is one of the surface boundary conditions:

$$U = V = W = 0 \quad (17)$$

Moreover, another boundary condition similar to no slip condition exists for surface temperature. If surface temperature is $T = T_w$, the temperature of the fluid in contact with the surface would be also T_w. For a given surface temperature, the boundary condition of the fluid temperature at contact with the surface will be written as:

$$T = T_w \quad (18)$$

If the surface temperature is unknown or in other words it varies based on the heat transfer upon time, the boundary condition will be determined by Fourier law of heat conduction:

$$\dot{Q}_w = -k \left.\frac{\partial T}{\partial n}\right)_w \quad (19)$$

Where n shows the surface perpendicular direction

If the thermal flux is zero, the surface will be called adiabatic for which the surface boundary condition will be defined as:

$$\left.\frac{\partial T}{\partial n}\right)_w = 0 \quad (20)$$

3.2.2. Boundary condition in microchannels

The ratio of mean molecular path to the container specific length of microchannels is called Knudsen number:

$$\mathrm{Kn} = \frac{\lambda}{D_h} \quad (21)$$

Knudsen number is applied for classification of flow; if Knudsen number lies in the range of $0.001 \leq \mathrm{Kn} \leq 0.1$, then the flow regime is slipping. This means that the condition of no slip velocity and no temperature jump on the walls do not hold anymore. This condition mainly occurs in

microchannels [23]. The condition of slip velocity on the walls is as follows [24]:

$$\mathrm{U_f} - \mathrm{U_W} = \lambda \frac{2-\sigma}{\sigma} \frac{\partial \mathrm{U}}{\partial \mathrm{n}} \tag{22}$$

Temperature jump condition has the following form [25]:

$$_{\mathrm{f}} - _{\mathrm{W}} = \frac{2-\sigma_{\mathrm{t}}}{\sigma_{\mathrm{t}}} \frac{2\gamma}{\gamma+1} \frac{\lambda}{\mathrm{Pr}} \frac{\partial}{\partial \mathrm{n}} \tag{23}$$

where λ is the tangential momentum coefficient generally in the range of 0.87-1. γ value is usually considered as 1.04 [26]. In this study, 1 and 1.04 were considered for λ and γ, respectively. σ_t denotes thermal friction coefficient which varies in the range of 0.32-1 which was considered as 1 in this study.

3.3. Discretization of time dependent terms of flow equations

Methods like Taylor method have simple concept. But calculation of successive derivations is frustrating and time consuming as it requires calculation of higher order derivatives. To avoid the need for higher order derivatives, Range- Kutta method can calculate the desired function in more points and has the same accuracy as Taylor method. In this content, fourth-order Range-Kutta method has high accuracy. Its general form is:

$$\begin{aligned}
k_1 &= hf\left(X_i, Y_i\right) \\
k_2 &= hf\left(X_i + \frac{h}{2}, Y_i + \frac{k_1}{2}\right) \\
k_3 &= hf\left(X_i + \frac{h}{2}, Y_i + \frac{k_2}{2}\right) \\
k_4 &= hf\left(X_i + h, Y_i + k_3\right) \\
Y_{i+1} &= Y_i + \frac{1}{6}\left(k_1 + 2k_2 + 2k_3 + k_4\right)
\end{aligned} \tag{24}$$

For example, continuity equation temporal terms quantization by Range Kutta method will result in:

$$\begin{aligned}
kP_1 &= hf\left(\zeta_{i,j}, U_{i,j}, V_{i,j}, P_{i,j}\right) \\
kP_2 &= hf\left(\zeta_{i,j} + \frac{h}{2}, U_{i,j} + \frac{kU_1}{2}, V_{i,j} + \frac{kV_1}{2}, P_{i,j} + \frac{kP_1}{2}\right) \\
kP_3 &= hf\left(\zeta_{i,j} + \frac{h}{2}, U_{i,j} + \frac{kU_2}{2}, V_{i,j} + \frac{kV_2}{2}, P_{i,j} + \frac{kP_2}{2}\right) \\
kP_4 &= hf\left(\zeta_{i,j} + h, U_{i,j} + kU_3, V_{i,j} + kV_3, P_{i,j} + kP_3\right) \\
\frac{dP}{d\xi} &= f\left(\zeta_{i,j}, U_{i,j}, V_{i,j}, P_{i,j}\right)
\end{aligned} \tag{25}$$

In the above equation, the values of each kP will be determined by substitution in continuity equation:

$$kP_1 = \frac{\beta h}{2A} \begin{pmatrix}
-\left(U_{i,j} + U_{i,j-1}\right)\left(Y_{i+1,j} - Y_{i,j}\right) - \left(U_{i,j} + U_{i+1,j}\right)\left(Y_{i+1.j+1} - Y_{i+1,j}\right) \\
-\left(U_{i,j} + U_{i,j+1}\right)\left(Y_{i,j+1} - Y_{i+,j+1}\right) - \left(U_{i,j} + U_{i-1,j}\right)\left(Y_{i,j} - Y_{i,j+1}\right) \\
+\left(V_{i,j} + V_{i,j-1}\right)\left(X_{i+1,j} - X_{i,j}\right) + \left(V_{i,j} + V_{i+1,j}\right)\left(X_{i+1.j+1} - X_{i+1,j}\right) \\
+\left(V_{i,j} + V_{i,j+1}\right)\left(X_{i,j+1} - X_{i+,j+1}\right) + \left(V_{i,j} + V_{i-1,j}\right)\left(X_{i,j} - X_{i,j+1}\right)
\end{pmatrix} \tag{26}$$

$$kP_2 = \frac{\beta h}{2A} \begin{pmatrix}
-\left(\left(U_{i,j} + \frac{kU_1}{2}\right) + U_{i,j-1}\right)\left(Y_{i+1,j} - Y_{i,j}\right) + \left(\left(U_{i,j} + \frac{kU_1}{2}\right) + U_{i+1,j}\right)\left(Y_{i+1.j+1} - Y_{i+1,j}\right) \\
-\left(\left(U_{i,j} + \frac{kU_1}{2}\right) + U_{i,j+1}\right)\left(Y_{i,j+1} - Y_{i+,j+1}\right) - \left(\left(U_{i,j} + \frac{kU_1}{2}\right) + U_{i-1,j}\right)\left(Y_{i,j} - Y_{i,j+1}\right) \\
+\left(\left(V_{i,j} + \frac{kV_1}{2}\right) + V_{i,j-1}\right)\left(X_{i+1,j} - X_{i,j}\right) + \left(\left(V_{i,j} + \frac{kV_1}{2}\right) + V_{i+1,j}\right)\left(X_{i+1.j+1} - X_{i+1,j}\right) \\
+\left(\left(V_{i,j} + \frac{kV_1}{2}\right) + V_{i,j+1}\right)\left(X_{i,j+1} - X_{i+,j+1}\right) + \left(\left(V_{i,j} + \frac{kV_1}{2}\right) + V_{i-1,j}\right)\left(X_{i,j} - X_{i,j+1}\right)
\end{pmatrix} \tag{27}$$

$$kP_3=\frac{\beta h}{2A}\begin{pmatrix}-\left(\left(U_{i,j}+\frac{kU_1}{2}\right)+U_{i,j-1}\right)\left(Y_{i+1,j}-Y_{i,j}\right)+\left(\left(U_{i,j}+\frac{kU_1}{2}\right)+U_{i+1,j}\right)\left(Y_{i+1.j+1}-Y_{i+1,j}\right)\\-\left(\left(U_{i,j}+\frac{kU_2}{2}\right)+U_{i,j+1}\right)\left(Y_{i,j+1}-Y_{i+,j+1}\right)-\left(\left(U_{i,j}+\frac{kU_2}{2}\right)+U_{i-1,j}\right)\left(Y_{i,j}-Y_{i,j+1}\right)\\+\left(\left(V_{i,j}+\frac{kV_2}{2}\right)+V_{i,j-1}\right)\left(X_{i+1,j}-X_{i,j}\right)+\left(\left(V_{i,j}+\frac{kV_2}{2}\right)+V_{i+1,j}\right)\left(X_{i+1.j+1}-X_{i+1,j}\right)\\+\left(\left(V_{i,j}+\frac{kV_2}{2}\right)+V_{i,j+1}\right)\left(X_{i,j+1}-X_{i+,j+1}\right)+\left(\left(V_{i,j}+\frac{kV_2}{2}\right)+V_{i-1,j}\right)\left(X_{i,j}-X_{i,j+1}\right)\end{pmatrix} \tag{28}$$

$$kP_4=\frac{\beta h}{2A}\begin{pmatrix}-\left(\left(U_{i,j}+kU_3\right)+U_{i,j-1}\right)\left(Y_{i+1,j}-Y_{i,j}\right)-\left(\left(U_{i,j}+kU_3\right)+U_{i+1,j}\right)\left(Y_{i+1.j+1}-Y_{i+1,j}\right)\\-\left(\left(U_{i,j}+kU_3\right)+U_{i,j+1}\right)\left(Y_{i,j+1}-Y_{i+,j+1}\right)-\left(\left(U_{i,j}+kU_3\right)+U_{i-1,j}\right)\left(Y_{i,j}-Y_{i,j+1}\right)\\+\left(\left(V_{i,j}+kV_3\right)+V_{i,j-1}\right)\left(X_{i+1,j}-X_{i,j}\right)+\left(\left(V_{i,j}+kV_3\right)+V_{i+1,j}\right)\left(X_{i+1.j+1}-X_{i+1,j}\right)\\+\left(\left(V_{i,j}+kV_3\right)+V_{i,j+1}\right)\left(X_{i,j+1}-X_{i+,j+1}\right)+\left(\left(V_{i,j}+kV_3\right)+V_{i-1,j}\right)\left(X_{i,j}-X_{i,j+1}\right)\end{pmatrix} \tag{29}$$

$$P_{i+1}=P_i+\frac{1}{6}\left(kP_1+2kP_2+2kP_3+kP_4\right) \tag{30}$$

3.4. Nusslet number

Local Nusslet number of the nanofluids is defined as:

$$\mathrm{Nu}=-\frac{\mathrm{k_{nf}}}{\mathrm{k_f}}\frac{\partial\theta}{\partial\mathrm{n}} \tag{31}$$

where n represents the surface perpendicular direction.

Local Nusslet number on vertical and horizontal walls can be defined as:

$$\mathrm{Nu_x}=-\frac{\mathrm{k_{nf}}}{\mathrm{k_f}}\frac{\partial\theta}{\partial\mathrm{Y}}$$
$$\mathrm{Nu_y}=-\frac{\mathrm{k_{nf}}}{\mathrm{k_f}}\frac{\partial\theta}{\partial\mathrm{X}} \tag{32}$$

Mean Nusslet number of this problem can be obtained by integrating local Nusslet number on the warm walls as:

$$\overline{\mathrm{Nu}}=\frac{1}{\mathrm{h}+(1-\mathrm{w})}\left(\int_0^{\mathrm{h}}\mathrm{Nu_y}+\int_{\mathrm{w}}^{1}\mathrm{Nu_x}\right) \tag{33}$$

3.5. Problem solving algorithm

Time marching method was used to solve Navier-Stokes and energy equations. The stable state equation was converted to an unstable one and therefore it is possible to virtually progress in time. To break the spatial terms, finite volume method was used while fourth-order Range-Kutta method was employed for temporal terms. General trend of problem solving is as follows: first an initial velocity and temperature will be guessed for all terms in all points. Convection and viscose terms will be separately broken by finite volume method and these initial guesses will be inserted in them (it must be noted that as mentioned before, 4^{th} -order Range-Kutta method was employed). After inserting the initial guesses for the known values of velocity, temperature and pressure in time n, their new values for time (n+1) will be obtained and this trend will be continued. In fact, after each iteration, the obtained values of velocity, temperature and pressure will be better approximations for the stable state solution.

4. Results

4.1. Validation

To confirm the validity of the applied numerical method and written code, the independence of meshing and comparison of the obtained results with the available results in the literature were done. The present problem was run for a definite situation for 4 different meshing (50×50, 100×100, 150×150, 200×200) and it was observed that the maximum difference of Nusslet numbers is less than

1.5%. Therefore, 100×100 meshing was selected to save time and also maintain the accuracy of the calculations. As mentioned before, no study was conducted on nanofluid flow in Γ-shaped microchannels; hence, to ensure the validity of the written code, the mentioned code was run for Kn=0 which corresponded to nanofluid flow in a Γ-shaped channel with ordinary dimensions. Then the results were compared with those in Ref. [27]; and it was observed that the results completely coincided.

In addition, the effects of Grashof number variation and nanoparticles diameter non-uniformity of nanofluid flow, isotherm lines, velocity field and Nusslet number will be investigated.

4.2. Isothem lines

4.2.1. Grashof number effect on isotherm lines

Isotherm lines are plotted for Grashof numbers of 10^2-10^5 at dp=5nm and Kn=0.001(Figs. 2-4).

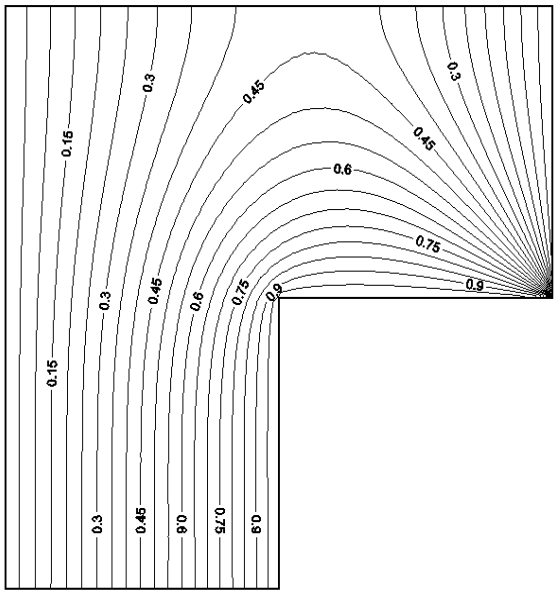

Fig. 2. Isotherm lines for $\mathbf{Gr = 10^2}$ and Kn=0.001.

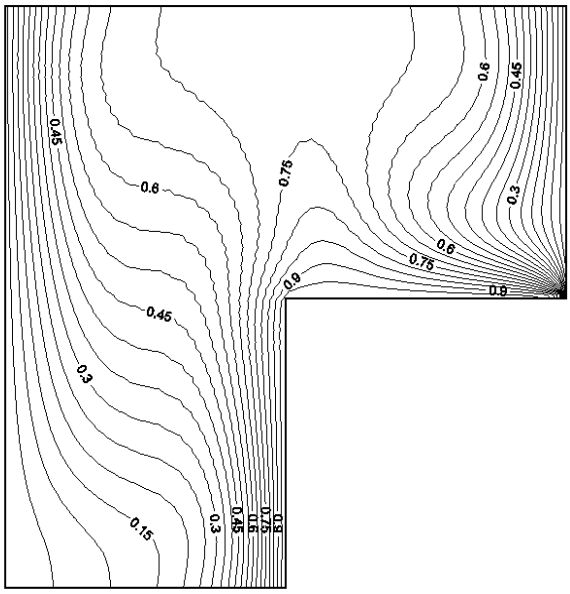

Fig. 3. Isotherm lines for Gr=10^4 and $\mathbf{Kn = 0.001}$.

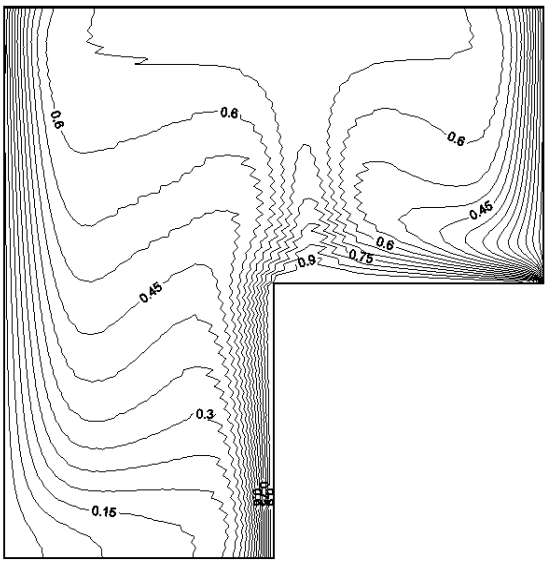

Fig. 4. Isotherm lines for Gr=10^5 and $\mathbf{Kn = 0.001}$.

As we know, heat transfer in natural convection phenomenon is the result of density gradient due to increase of temperature gradient. The results show that for $Gr = 10^2$, isotherm lines are approximately direct and vertical lines; in such situation, heat transfer between the two walls is due to convection. However, for $Gr = 10^5$, isotherm lines are compacted near the isotherm walls which is the result of density gradient near the walls. Heat transfer between the warm and cold walls is mainly due to convection. These results are in accordance with the fact that at higher Grashof numbers, heat transfer will be carried out between warm and cold walls via convection.

4. 2. 2. Effect of nanoparticles diameter non-uniformity on isotherm lines

To investigate the effect of nanoparticles diameter non-uniformity on different parameters, variable of R was defined as the ratio of minimum nanoparticle diameter to its maximum:

$$R = \frac{d_{p,min}}{d_{p,max}} \tag{34}$$

Figures 5-7 show isotherm lines for $Gr = 10^4$, dp=5 nm, kn=0.01 and $\phi = 0.05$ for different values of R.

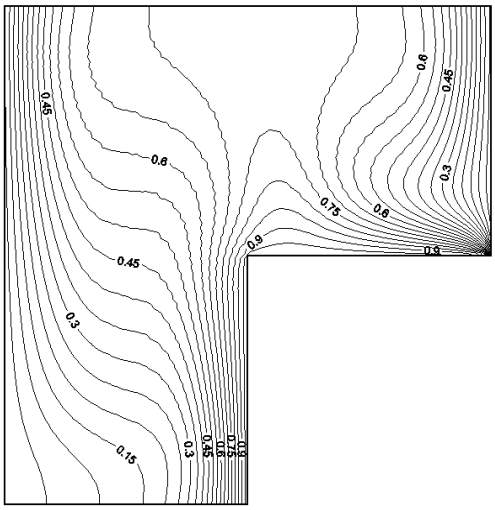

Fig. 5. Isotherm lines for $\mathbf{Kn = 0.01}$, Gr=10^4 , $\boldsymbol{\phi = 0.05}$ and $\mathbf{R = 0.001}$.

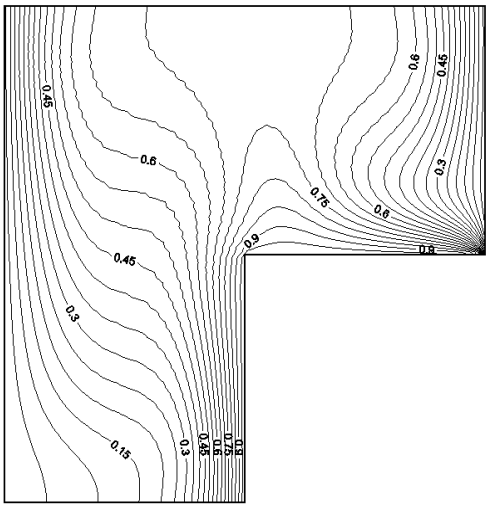

Fig. 6. Isotherm lines for $\mathbf{Kn = 0.01}$, Gr=10^4 , $\boldsymbol{\phi = 0.05}$ and $\mathbf{R = 0.004}$.

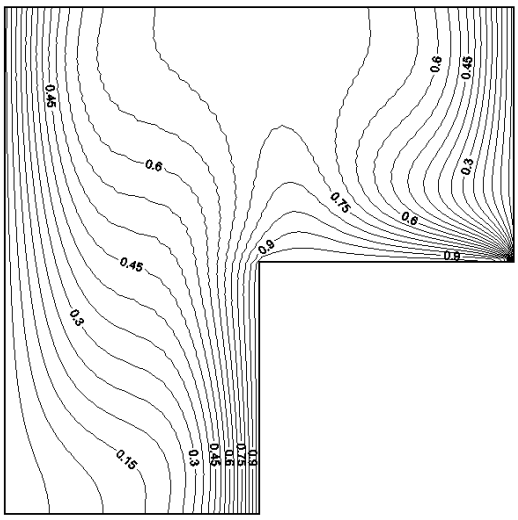

Fig. 7. Isotherm lines for $\mathbf{Kn = 0.01}$, Gr=10^4 , $\boldsymbol{\phi = 0.05}$ and $\mathbf{R = 0.008}$.

As can be seen in the figures, increase in R, will increase isotherm lines distortion to some extent.

4. 3. Velocity vectors

In Figs. 8 and 9, velocity vectors are shown for $\mathrm{Gr} = 10^3$ and $\mathrm{Gr} = 10^5$ in dp=5nm and Kn=0.001; as indicated in the figures, two rotational cells were created inside the container. The cell in the left side is larger and rotates anticlockwise which is mostly due to the effect of left-side cold vertical wall and right-side warm vertical wall. The right-side cell is smaller and rotates clockwise which is more under the influence of right-side cold vertical wall and warm horizontal wall. As can be observed, the rotation direction of both cells is from the warm to cold wall as anticipated.

It can be seen that increase in Grashof number would result in larger velocity vectors. As increase in the Grashof number implies increase in bouyancy force and reinforcement of convection flow, increase of velocity vectors by enhancement of Grashof number completely coincides with the physical background of the problem.

Given that the flow lines have more quantitative form in comparison with the velocity vectors, the flow lines will be investigated in more details.

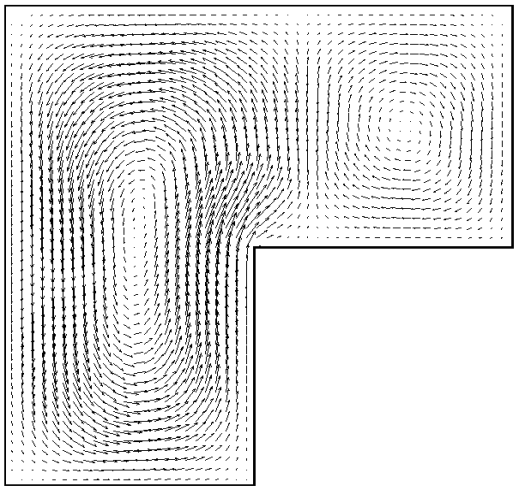

Fig. 8. Velocity vectors for Gr=10^3 and $\mathbf{Kn = 0.001}$.

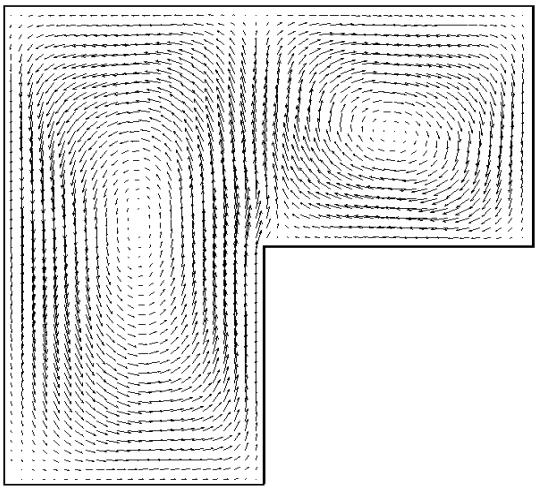

Fig. 9. Velocity vectors for Gr=10^5 and $\mathbf{Kn = 0.001}$.

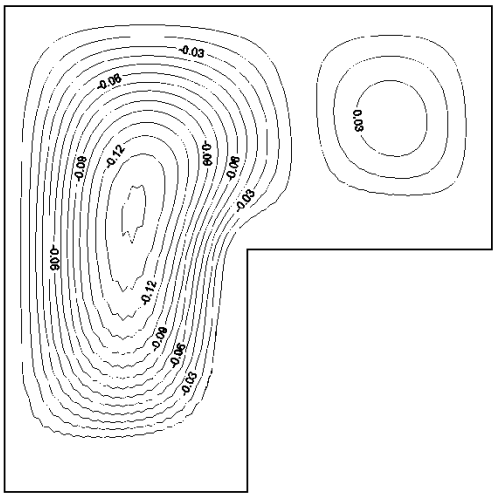

Fig. 10. Stream lines for Gr=10^2 and $\mathbf{Kn = 0.001}$.

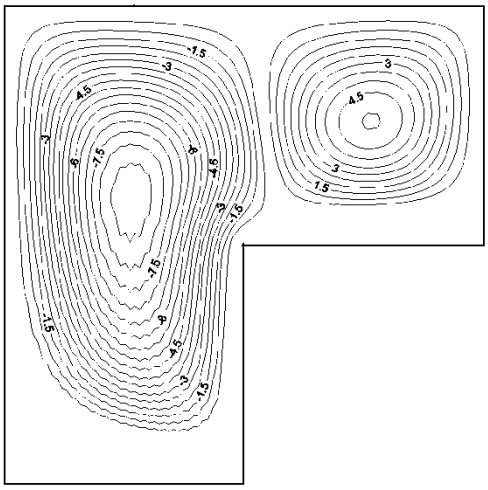

Fig. 11. Stream lines for Gr=10^4 and $\mathbf{Kn = 0.001}$.

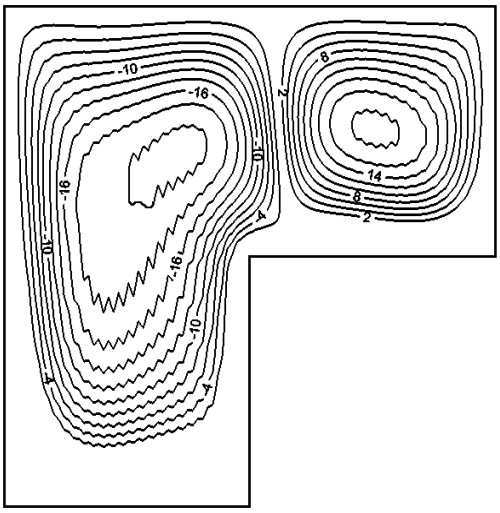

Fig. 12. Stream lines for Gr=10^5 and $\mathbf{Kn = 0.001}$.

4. 4. Stream lines

4. 4. 1. Effect of Grashof number on stream lines

Stream lines are plotted for $Gr = 10^2$ to $Gr = 10^5$ in dp=5 nm and Kn=0.001.

As can be seen, two rotational cells were created inside the channel; the cell in the left side is larger and the one in the right side is smaller. Increase in Grashof number will increase bouyancy force and create stronger rotation inside the channel.

4. 5. Effect of variation in different parameters on Nusslet number

4. 5. 1. Effect of Grashof number on Nusslet number

As we know, Nusslet number shows the ratio of convective to conductive heat transfer. Therefore, it is evident that Nusslet number should increase with increase in Grashof number, as increase in Grashof number will make the velocity vectors larger giving rise to stronger rotation inside the channel. Hence the contribution of convection heat transfer will become more highlighted. Fig. 13 clearly shows this issue.

4. 5. 2. Effect of R on Nusslet number

As shown in Fig. 14, increase in R parameter from 0.001 to 0.008, increased Nusslet number by 20.1 and 15.1% in $Gr = 10^2$ and $Gr = 10^5$, respectively.

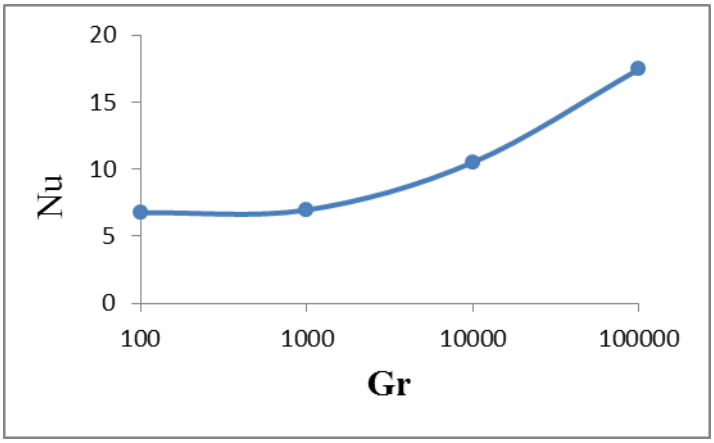

Fig. 13. Effect of Grashof number on Nusslet number.

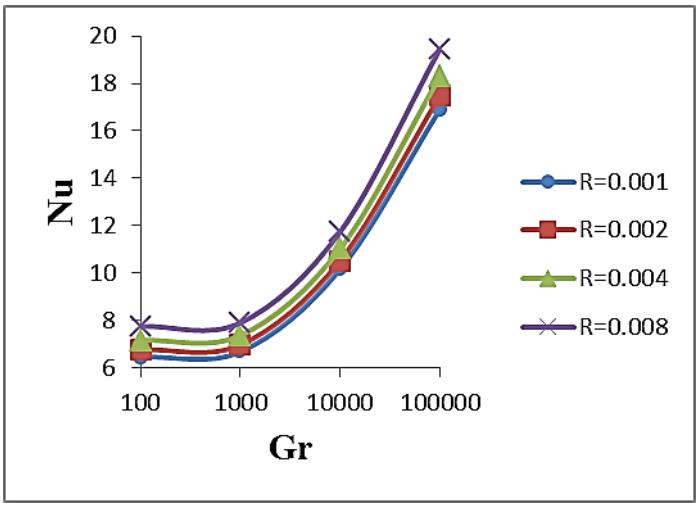

Fig. 14. Effect of R parameter on Nusslet number.

5. Conclusions

In the present study, finite-volume procedure was presented for solving the natural convection of the laminar Al_2O_3/Water nanofluid flow in a Γ shaped microchannel. Results showed that at low Grashof numbers, isotherm lines are vertical and direct while for higher Grashof numbers, isotherm lines are more compact and accumulated near the isotherm walls. Increase in Grashof number will result in larger velocity vectors. Increase in Grashof number will increase bouyancy force, giving rise to stronger rotation inside the channel. Increase in Grashof number will enhance heat transfer and Nusslet number. Increase in R will increase compaction and distortion of isotherm lines and also the heat transfer.

References

[1] Dagtekin I., Oztop H. F., Natural Convection Heat Transfer by Heated Partitions within Enclouser, Heat Mass Transfer (2001) 28(6): 823-834.

[2] Masuda H., Ebata A. , Teramae K., Hishinuma N. , Alteration of Thermal Conductivity and Viscosity of Liquid by Dispersing Ultra-Fine Particles (Dispersions of -Al2O3, SiO2, and TiO2 Ultra-Fine Particles) Netsu Bussei (Japanese) (1993) 4: 227–233.

[3] Eastman J. A. , Choi S. U. S. , Li S., Yu W., Thompson L.J., Anomalously Increased Effective Thermal Conductivities of Ethylene Glycol Based Nanofluids Containing Copper Nanoparticles, Applied Physics Letters (2001) 78: 718–720.

[4] Xie H., Wang J., Xi T. , Liu Y., Ai F., Dependence of the Thermal Conductivity of Nanoparticle–Fluid Mixture on the Base Fluid, Journal of Materials Science Letters (2002) 21: 1469–1471.

[5] Xie H., Wang J., Xi T. , Liu Y., Ai F., Thermal Conductivity Enhancement of Suspensions Containing Nanosized Alumina Particles, Journal of Applied Physics (2002) 91: 4568–4572.

[6] Wang B. X., Li H., Peng X.F. , Research on the Heat-Conduction Enhancement for Liquid with Nanoparticle Suspensions, Journal of Thermal Science (2002)11 (3): 214–219.

[7] Das S. K., Putra N., Thiesen P., Roetzel W., Temperature Dependence of Thermal Conductivity Enhancement for Nanofluids, Journal of Heat Transfer (2003) 125: 567–574.

[8] Zhang H., Shao S., Xu H., Tian C., Heat Transfer and Flow Features of Al2O3-Water Nanofluids Flowing Through a Circular Microchannel – Experimental Results and Correlations, Applied Thermal Engineering (2013) 61: 86-92.

[9] Arie M., Shooshtari A., Dessiatoun S., Al-Hajri E., Ohadi M., Numerical Modeling and Thermal Optimization of a Single-Phase Flow Manifold-Microchannel Plate Heat Exchanger, International Journal of Heat and Mass Transfer (2015) 81: 478-89.

[10] Ebrahimi A., Roohi E., Kheradmand S., Numerical Study of Liquid Flow and Heat Transfer in Rectangular Microchannel with

Longitudinal Vortex Generators, Applied Thermal Engineering (2014)78: 576-83.

[11] Yue Y. , Mohammadian S. K., Zhang Y., Analysis of Performances of a Manifold Microchannel Heat Sink with Nanofluids, International Journal of Thermal Sciences (2015) 89: 305- 13.

[12] Hedayati F., Domairry G., Effects of Nanoparticle Migration and Asymmetric Heating on Mixed Convection of TiO 2–H2O Nanofluid Inside a Vertical Microchannel, Powder Technology (2015) 272: 250-59.

[13] Zhu X. W., Fu Y. H., Zhao J. Q., Zhu L., Three-Dimensional Numerical Study of the Laminar Flow and Heat Transfer in a Wavy-Finned Heat Sink Filled with Al2O3/ethylene Glycol-Water Nanofluid, Numerical Heat Transfer Part A: Applications (2015)1-14.

[14] Yang Y. T., Wang Y. H., Tseng P. K., Numerical Optimization of Heat Transfer Enhance- 531 Ment in a Wavy Channel Using Nanofluids, International Communications in Heat and Mass Transfer (2014) 51 (532): 9-17

[15] Esfahanian V., Akbarzadeh P., The Jameson's Numerical Method for Solving the Incompressible Viscous and Inviscid Flows by Means of Artificial Compressibility and Preconditioning Method, Applied Mathematics and Computation (2008) 206:651-661.

[16] Chorin A. J., A Numerical Method for Solving Incompressible Viscous Flow Problems, Journal of Computational physics(1997) 112: 118-125.

[17] Bassi F., Crivellini A., Pietro D. A., Rebay S., An Artificial Compressibility Flux for the Discontinuous Galerkin Solution of the Incompressible Navier-Stokes Equations, Journal of Computational Physics(2006) 218:794-815.

[18] Jang S. P., Lee J. H., Hwang K. S., Choi S. U. S., Particle Concentration and Tube Size Dependence of Viscosities of Al2O3-Water Nanofluids Flowing Through Micro- and Mini Tubes, Applied Physics Letters (2007) 91: 243112.

[19] Hamilton R. L., Crosser O. K., Thermal Conductivity of Heterogeneous Two Component Systems, Journal of Industrial & Engineering Chemistry Fundamentals (1962) 1: 187–191.

[20] Xu J. , Yu B., Zou M. , Xu P., A New Model for Heat Conduction of Nanofluids Based on Fractal Distributions of Nanoparticles, The Journal of Physics D (2006) 39:4486–4490.

[21] Chorin A. J., A Numerical Method for Solving Incompressible Navier-Stokes Equations, The Journal of Computational Physics (1967) 2: 12-26.

[22] Ohwada T., Asinari P., Artificial Compressibility Method Revisited: Asymptotic Numerical Method for Incompressible Navier-Stokes Equations, Journal of Computational Physics (2010) 229: 1698-1723.

[23] Beskok A., Karniadakis G. E., Simulation of Heat and Momentum Transfer in Complex Micro –Geometries, Journal of Thermophysics and Heat Transfer (1994) 8:355 –370.

[24] Zhang T., Jia L., Yang L., Jaluria Y., Effect of Viscous Heating on Heat Transfer Performance in Microchannel Slip Fow Region, International Journal of Heat and Mass Transfer (2010) 53: 4927 –4934.

[25] Shojaeian M., Dibaji R., Three-Dimensional Numerical Simulation of the Slip Flow Through Triangular Microchannels, International Communications in Heat and Mass Transfer (2010) 37: 324-329.

[26] Harley J., Huang Y., Bau H., Zemel J. N., Gas Flows in Micro-Rohsenow W. M., and Choi H. Y., 1961, Heat, Mass, and Momentum Transfer, Prentice-Hall, Englewood Cliffs, Chapter 11(1995).

[27] Dehnavi R., Rezvani A., Numerical Investigation of Natural Convection Heat Transfer of Nanofluids in a Γ Shaped Cavity, Superlattices and Microstructures (2012) 52:312–325